J. Fluid Mech. (1978), *vol.* 85, *part* 3, *pp.* 497–518
Printed in Great Britain

Laser anemometer study of flow development in curved circular pipes

By Y. AGRAWAL, L. TALBOT AND K. GONG
Department of Mechanical Engineering, University of California, Berkeley

(Received 12 October 1976 and in revised form 2 August 1977)

An experimental investigation was carried out of the development of steady, laminar, incompressible flow of a Newtonian fluid in the entry region of a curved pipe for the entry condition of uniform motion. Two semicircular pipes of radius ratios $\frac{1}{20}$ and $\frac{1}{7}$ were investigated, covering a Dean number range from 138 to 679. The axial velocity and the component of secondary velocity parallel to the plane of curvature of the pipe were measured using laser anemometry. It was observed that, in the upstream region where the boundary layers are thin compared with the pipe radius, the axial velocity within the irrotational core first develops to form a vortex-like flow. In the downstream region, characterized by viscous layers of thickness comparable with the pipe radius, there appears to be three-dimensional separation at the inner wall. There is also an indication of an additional vortex structure embedded within the Dean-type secondary motion. The experimental axial velocity profiles are compared with those constructed from the theoretical analyses of Singh and Yao & Berger. The quantitative agreement between theory and experiment is found to be poor; however, some of the features observed in the experiment are in qualitative agreement with the theoretical solution of Yao & Berger.

1. Introduction

The problem of flow development in curved pipes is one of fundamental interest in fluid mechanics. Although considerable effort has gone into the study of fully developed flows in curved pipes, the problem of flow development has only recently received comparable attention, in part owing to its relevance to such arterial phenomena as the mixing of injected substances and the distribution of wall shear, which has been conjectured to be linked to atherogenesis by Caro (1973), Fry (1973) and others. The present study reports the results of an experimental investigation of this flow development.

The secondary motion in the fully developed as well as in the entry region of curved pipes is usually explained on the basis of centrifugally induced pressure-gradient considerations as, for example, in the second paper of Dean (1928). In the following, an alternative description of the flow development process is given in terms of vorticity arguments which will be of help in interpreting the results of our measurements. The co-ordinate systems are shown in figure 1(*a*). We shall employ the terms 'circular motion' and 'circumferential motion' to denote, respectively, motion in the streamwise and ψ directions.

We may imagine a vortex ring, concentric with and of only slightly smaller diameter than the pipe, as being representative of the vorticity within the very thin boundary

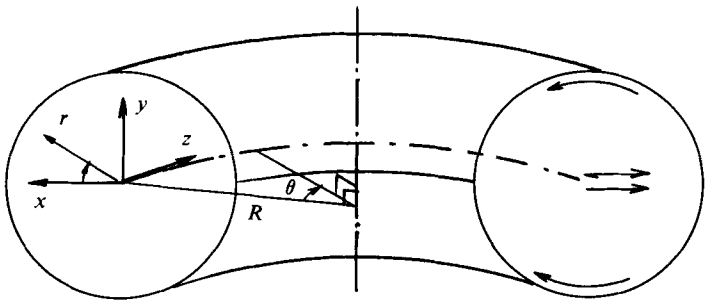

(*a*)

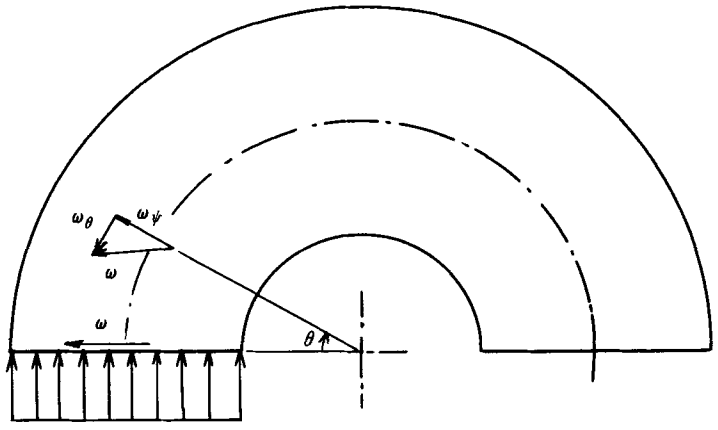

(*b*)

FIGURE 1. (*a*) Co-ordinate systems. (*b*) Transport of a vortex line in the lower half of pipe.

layer which has formed just downstream of the entrance to the pipe. Initially, the vorticity represented by this vortex ring has only one component, ω_ψ, as indicated in figure 1 (*b*). Consider now the transport of this vortex line, which being a material line moves at the local fluid velocity. In a time Δt, the segments of this vortex line travel nearly equal linear distances of order $\overline{W}\Delta t$, $\overline{W}$ being the average streamwise velocity. Thus segments of this vortex line near the inner wall travel through a greater angular distance θ than those near the outer wall. The vorticity vector, being tangential to this vortex line, now in general has two components, ω_ψ and ω_θ, the latter being the streamwise vorticity, as shown in figure 1 (*b*), which induces outward motion exterior to the boundary layer. The presence of this ω_θ, however, results in the production, at the pipe wall, of vorticity of the opposite sign (see Lighthill 1963), which leads to circumferential motion in the boundary layer, from the outside of the bend to the inside of the bend.

The production of ω_θ due to convective bending, being proportional to $\sin\psi$, is evidently strongest at the pipe top and bottom walls ($\psi = \frac{1}{2}\pi, \frac{3}{2}\pi$). It is therefore to be expected that the circumferential motion would also be strongest here. The induced circumferential motion has the further effect of stretching vortex lines near the outer

wall, thus intensifying ω_ψ and keeping the boundary layer thin, while at the same time relaxing them in the inner wall region and causing a thickening of the boundary layer there. The circumferential motion also causes the outer wall to behave in the manner of a sink, drawing fluid from the core, which in turn counters the diffusive growth of the boundary layer there. At the inner wall, in opposite manner, the boundary-layer diffusive growth is augmented by source-like behaviour induced by the secondary motion.

We turn our attention now to the initial stages of flow development within the inviscid core. Since uniform streamwise motion does not constitute a solution to the inviscid flow problem in the toroidal geometry under consideration, an initially uniform core flow must progress towards its asymptotic ($\theta = \infty$) limit, the potential line vortex, which has a core velocity distribution of $W = \text{constant}/(R + r\cos\psi)$. The core will thus have a tendency to develop a streamwise velocity maximum near the inner wall, contrary to the fully developed flow case. This requires streaming motion of the secondary flow towards the inner wall in the core, exactly as in the boundary layer. Until thickening boundary layers overpower this tendency, the wall shear will be greater at the inner wall than at the outer wall. Interestingly, the development of the core inviscid vortex has not been anticipated by previous workers. It is perhaps worth remarking that the mass flux associated with the secondary motion is not conserved in the developing flow, since the secondary flow streamlines do not become closed until the flow is fully developed.

Although there have been many theoretical and experimental investigations of fully developed flow in curved pipes (see Collins & Dennis (1975) for a recent bibliography) relatively little information is available on the entry-flow problem. The two theoretical investigations with which comparisons will be made are the analyses of Singh (1974) and Yao & Berger (1975). One other related study is that by Smith (1976) of the transition of Poiseuille flow from a straight pipe into a curved one. However, the solution obtained by Smith is valid only for very small curvature $\alpha \cong O(Re^{-2})$, where Re is the Reynolds number based on the pipe radius a, the mean velocity $\overline{W}$ and the kinematic viscosity ν ($Re = \overline{W}a/\nu$), and thus this solution cannot be compared usefully with the present results.

2. The experiment

A brief description of the major features of the experimental apparatus will be given. Further details can be found in the report by Agrawal (1975).

The flow system

Figure 2 shows a schematic diagram of the flow system employed for the study. Two constant-level reservoirs at a differential elevation of approximately 2·5 m, connected to a recirculating pump, provided a steady flow. Flow straightening was carried out in a 30 cm diameter stagnation chamber using a multiple orifice plate and a wire screen. The circulating liquid was continuously filtered, but a partial bypass of the filter was provided to reduce capture of particles added for laser anemometry. The stagnation chamber was connected to the curved pipes by means of a trumpet-shaped inlet contraction section of empirical design.

Two curved pipes were studied. These both had an internal diameter of 1·5 in. but differed in radius ratio $\alpha = a/R$, one having $\alpha = \frac{1}{20}$, the other $\alpha = \frac{1}{7}$. The pipes were

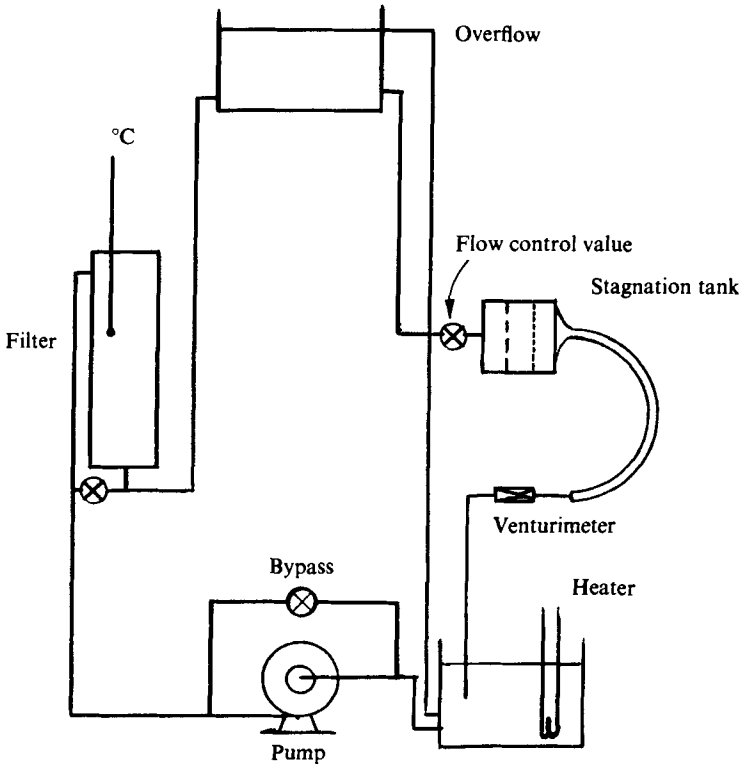

FIGURE 2. Schematic diagram of the flow facility.

machined out of Plexiglas in two halves, split at the plane of symmetry.† Both the circular internal and the planar external surface were polished carefully using a sequence of polishing pastes and wool cloths. The circulating liquid employed was a mixture of glycerin and water, in proportions chosen to match closely the index of refraction of Plexiglas. Exact matching was not possible, thus requiring refractive corrections in data processing, but approximate matching was required to ensure intersection of the laser beams within the flow. Careful smoothing and polishing of the inlet surfaces was carried out to ensure smooth laminar flow at the entrance to the pipes. The flow exited through a modest contraction of area ratio 4:1 into a venturimeter discharging into the lower reservoir.

Instrumentation and control

Although the actual flow rates used in computation of the Reynolds numbers were obtained by numerical integration of the measured axial velocity profiles, a venturimeter type flow sensor was also employed to monitor and maintain the flow rate constant to within $\pm 2\,\%$. A Hewlett-Packard differential pressure transducer of type

† This method of fabrication of the curved pipe served two purposes. It ensured that the internal machined cross-section of the pipe was accurately circular, in contrast to the coiled pipes used by other investigators, which most likely had some ellipticity in cross-section due to the coiling process. Since the fabrication method produced a pipe of circular cross-section contained within planar outer walls, the laser measurements were simplified because beam refractive corrections were required for only one curved interface.

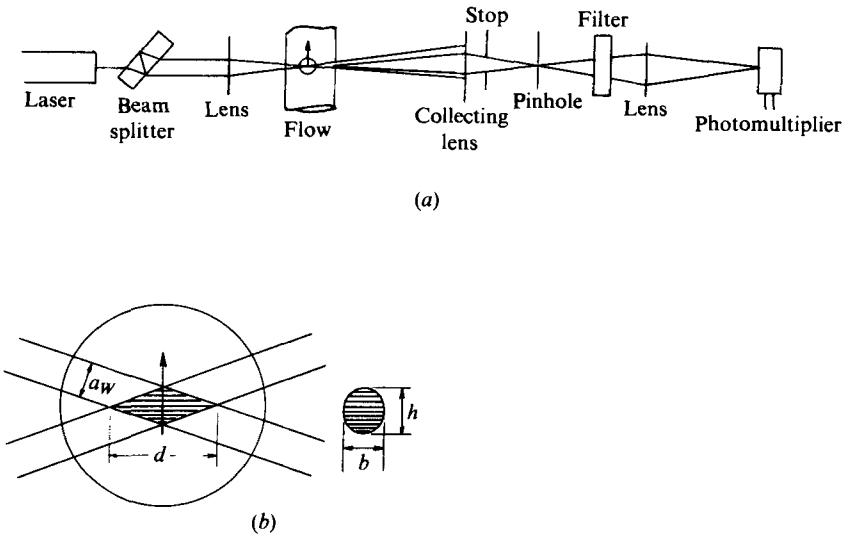

FIGURE 3. Schematic diagram of the laser-Doppler anemometer. (*a*) Fringe-mode LDA optics. (*b*) Details of probe volume.

267 BC powered by a 5 V, 24 kHz Schaevitz model SCM-025 source was used to sense the venturi pressure drop. A specially designed electronically controlled time-proportioning regulated heater was employed to keep the temperature of the circulating fluid constant to within $\pm 0{\cdot}2$ °C.

Velocity measurements at the entry section of the circular pipes were carried out by means of hot-film anemometry, because this region was inaccessible optically. A DISA model 55D01 anemometer was used with a TSI (Thermo-Systems, Inc., St Paul, Minn.) model 1210 hot-film probe.

The viscosity of the circulating liquid was measured using a Fann V-G Model 35 viscometer. The refractive index of the liquid was determined using a Pulfrich refractometer. Probable errors are estimated to be 5 % for the viscosity and 0·1 % for the refractive index.

All detailed fluid velocity measurements were carried out using a laser-Doppler anemometer operated in the fringe mode (see Durst, Melling & Whitelaw 1972). A schematic diagram of the LDA optics and signal processing electronics is shown in figure 3(*a*). For the axial velocity measurements the 15 mW He–Ne laser beam was split by an optical flat into two beams 1·93 cm apart and brought to intersection through the side of the pipe by a lens of focal length 55 mm. For the secondary velocity measurements the optical flat was replaced by a 15·24 cm diameter rotating bleached diffraction grating (Stevenson 1970) having 21 600 lines, which served the function both of a beam splitter and of a frequency shifter. Rotational speeds corresponding to frequency shifts of 20 kHz (for the lower Dean numbers) and 100 kHz (for the higher Dean numbers) were used, and a mirror–lens arrangement was used to bring the two first-order diffracted beams into intersection through the undersurface of the pipe. The probe volume dimensions, defined in figure 3(*b*), were estimated to be $a_W = b = 44\,\mu$m, $h = 45\,\mu m$ and $d = 256\,\mu$m for both beam-splitter arrangements. The LDA laser and optics were mounted on the x, y, z traverse of a milling machine with an accuracy of

traverse of 0·001 in. All of the optics mounted on this table were moved together to make velocity measurements at different points. Initially, 1 μm polystyrene spheres were used to seed the flow. However, Dow Chemical plastic paint Pigment 722 was found to be a much more economical and equally satisfactory seeding material, though less monodisperse in size. A typical relaxation time for these micron-sized particles in our flows was calculated to be of the order of 1 μs (Vom Stein & Pfeiffer 1972). Thus the particles could be expected to follow the flow velocity very closely.

The detection optics consisted of a 55 mm f/1·8 Pentax camera lens, a 0·3 mm diameter pinhole, a 30 Å bandpass interference filter centred at 6328 Å and an extended S-20 RCA type 4526 photomultiplier tube with a nominal 12 % quantum efficiency at 6328 Å. The amplified signal was frequency-demodulated on a TSI model 1090 LDA frequency tracker, which was independently checked for frequency calibration and linearity against a signal generator and a precision digital clock-counter. The accuracy was found to be within the manufacturer's specified limit of 0·4 % full scale.

Data acquisition and processing

Axial velocity measurements were made at five axial stations for each of the two curved pipes. Secondary velocity (i.e. the velocity U in the x direction of figure 1*a*) measurements were carried out at six axial stations within the $\alpha = \frac{1}{7}$ pipe. Owing to symmetry about the plane of the pipe axis, measurements are reported only in the lower halves of the pipes. (The symmetry condition was verified.) Velocity data were obtained along 'data lines'. These are defined as follows. For axial velocity measurements, the LDA optics were traversed at five different elevations, parallel to the symmetry plane. Owing to refraction of the laser beams, the actual measurement points lay on five straight lines making small angles with the symmetry plane. The y intersections (in inches) of these data lines with the outer wall of the pipe and their slopes dy/dx are recorded in the figure captions. For the secondary velocity measurements, the data lines were similarly slightly rotated away from the normal to the plane of symmetry, although in the plotted results these data lines are shown as vertical.

Individual axial velocity measurements are believed to be accurate to within 2 % and secondary velocities to within $\lesssim 5$ %. Flow rates at different axial stations obtained by integration of the axial velocity data were consistent to within 5 %.

3. Results and discussion

Measurements were first carried out at the pipe inlet by means of a hot-film probe to determine the nature of the inlet flow velocity profile. These data, obtained at two different values of Re for each of the two pipes, are displayed in figure 4. Since only relative values of the velocity were required, the probe output is reported in arbitrary units. It can be seen that the inlet velocity condition within the inviscid core is indeed the uniform flow case. We were not able to position the hot-film probe close enough to the pipe wall to obtain measurements within the very thin inlet boundary layer.

Axial velocity measurements were made by LDA for four different flow rates for pipe 1 ($\alpha = \frac{1}{20}$) and for three flow rates for pipe 2 ($\alpha = \frac{1}{7}$).The corresponding Dean numbers $\kappa = 2\alpha^{\frac{1}{2}}Re$ were 139, 200, 251 and 565 for pipe 1 and 183, 278 and 372 for pipe 2. Secondary velocity measurements were made within pipe 2 at three different flow rates corresponding to values of κ equal to 138, 205 and 679. For the purpose of

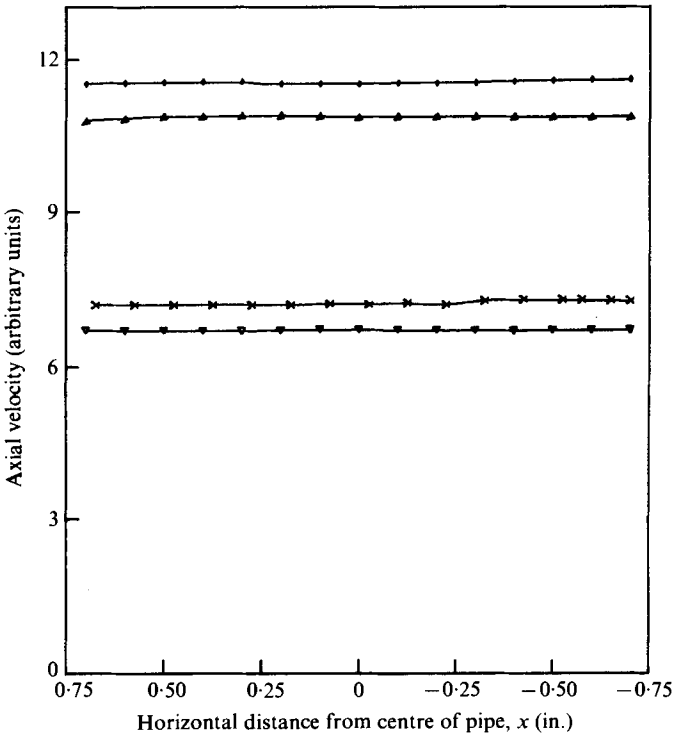

FIGURE 4. Inlet axial velocity profiles. Δ, $\alpha = \frac{1}{20}$, $Re \simeq 1200$; ∇, $\alpha = \frac{1}{20}$, $Re \simeq 300$; ◇, $\alpha = \frac{1}{7}$, $Re \simeq 500$; ×, $\alpha = \frac{1}{7}$, $Re \simeq 150$.

this paper we have selected as representative of the axial velocity data the case $\kappa = 565$ from pipe 1 (figures 5*a–e*) and $\kappa = 183$ from pipe 2 (figures 6*a–e*). Also, we have selected as typical of the results for the secondary velocity those for the Dean numbers $\kappa = 138$ and 679 (figures 9*a–f*, 10*a–f*).

More complete axial velocity data can be found in Agrawal's report. This report also contains secondary velocity data which were obtained before the frequency-shifting apparatus was available, and are therefore less accurate than the present secondary velocity data.

Discussion of the experimental results

From the axial velocity profiles in figures 5 and 6, it is immediately clear that qualitative differences in the flow field distinguish the 'upstream' and 'downstream' regions. The upstream region, immediately adjacent to the entry section, is characterized by thin boundary layers near the pipe wall and $\partial W/\partial y = 0$ in the core. However, in the direction parallel to the plane of symmetry, the streamwise velocity in the core increases very nearly linearly towards the centre of pipe curvature and the maximum axial velocity occurs near the inner wall. For a potential vortex, the quantity $G = (-a/W_0)(\partial W/\partial x)_0$ is equal to the radius ratio α, where the subscript zero denotes values at pipe centre-line. The values of G were estimated from our data to be 0·041, 0·045, 0·042 and 0·049 for pipe 1 at $\kappa = 139$, 200, 251 and 565, respectively, while for pipe 2 the value of G was 0·12 for all three cases, $\kappa = 183$, 278 and 372. Thus it appears that the vortex was fully developed, or very nearly so, by the time the flow reached our first observation station.

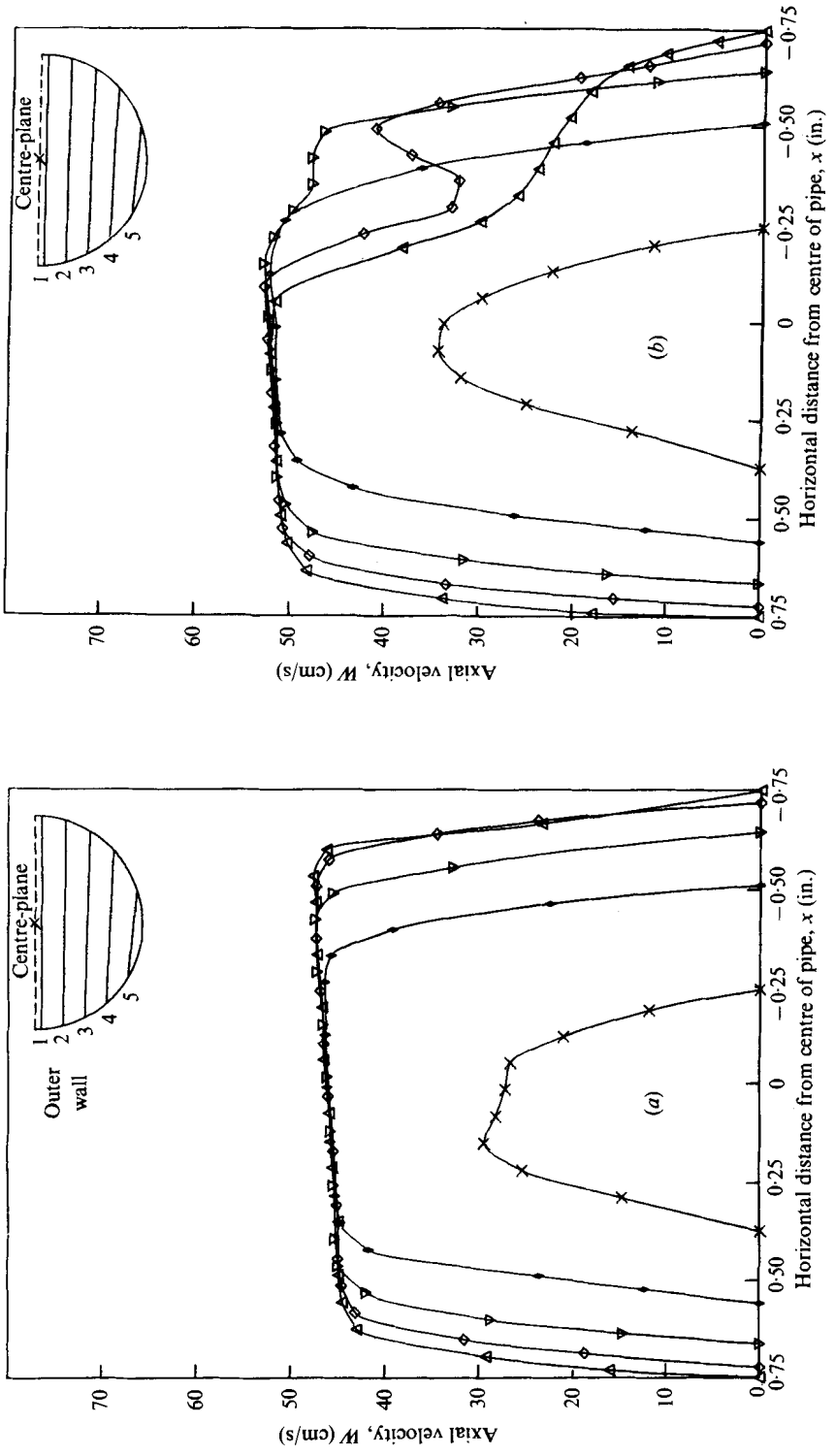

FIGURES 5(*a*, *b*). For legend see p. 506.

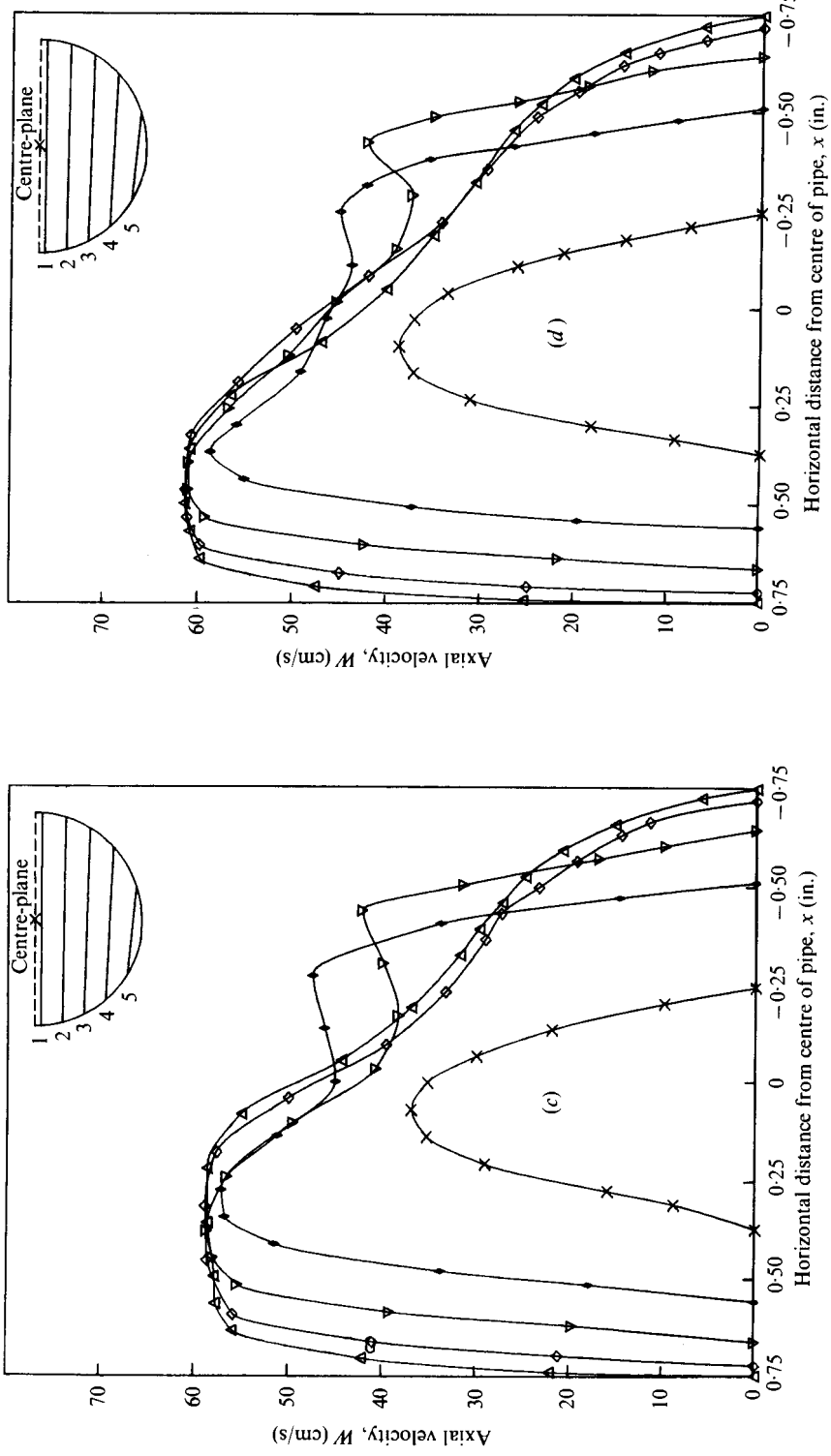

FIGURES 5(*c*, *d*). For legend see following page.

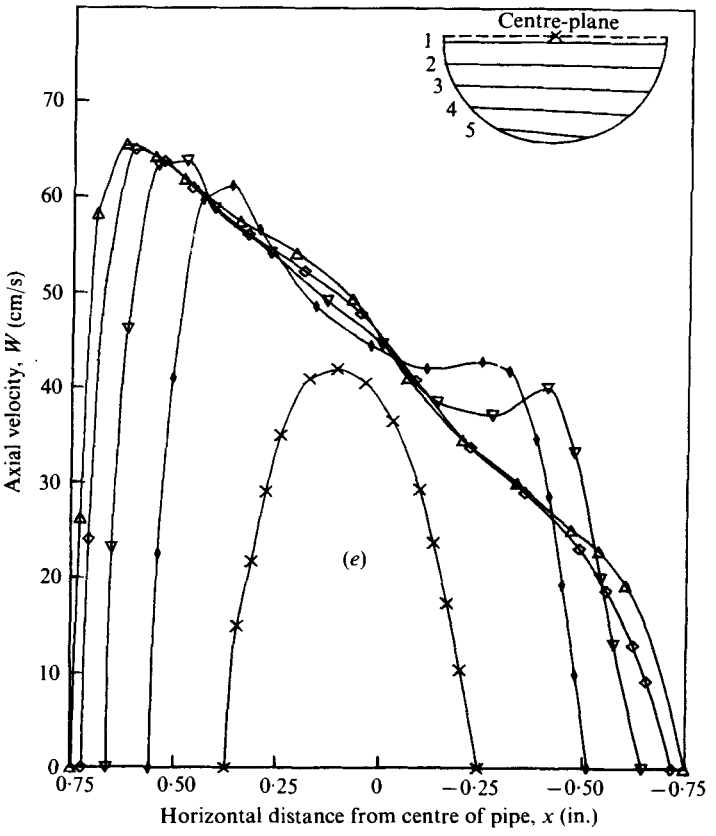

FIGURE 5. Axial velocity profiles for $\alpha = \frac{1}{20}$, $\kappa = 565$, $\overline{W} = 36{\cdot}1$ cm/s. (*a*) $l/a = 2{\cdot}4$, (*b*) $l/a = 12{\cdot}2$, (*c*) $l/a = 29{\cdot}4$, (*d*) $l/a = 37{\cdot}6$, (*e*) $l/a = 57{\cdot}6$. Profiles are shown along data lines 1–5. The initial values of y at the outer wall of the pipe for these lines, their slopes and the corresponding symbols are: (1) Δ, $-0{\cdot}050$, $-0{\cdot}0034$; (2) $\diamond$, $-0{\cdot}200$, $-0{\cdot}0141$; (3) ∇, $-0{\cdot}350$, $-0{\cdot}0270$; (4), $\blacklozenge$, $-0{\cdot}500$, $-0{\cdot}0465$; (5) $\times$, $-0{\cdot}650$, $-0{\cdot}0969$.

We now turn to the relatively more complex flow development in the 'downstream region', where the viscous-layer thickness, at least near the inner wall, is $O(a)$, as seen in figures 5(*b–e*) and 6(*b–e*). The remains of the inviscid core can be easily recognized by its vortex-like velocity distribution. It may be observed from figure 5(*b*) that a marked decrease in the axial velocity has occurred near the inner wall in the vicinity of data line 1, and that the smallest value of the velocity gradient dW/dx at the pipe wall occurs nearest the plane of symmetry. Also, data line 2 exhibits a clearly defined second maximum or peak in the axial velocity near the inner wall.

As the flow develops (figures 5*c–e*), one observes the continued erosion and velocity increase of the core region, while the second maximum appears progressively further away from the centre-plane, appearing at data lines 3 and 4 in figures 5(*c–e*), and at the same time becomes increasingly less pronounced. Far downstream (figure 5*e*), the axial velocity maximum appears on data line 1 near the outer wall. Within the streamwise distance available in our studies, the second maxima on data lines 3 and 4 did not disappear but did become diminished. It may be noted that doubly peaked velocity profiles observed here were also observed by Austin (1971) in his studies of the

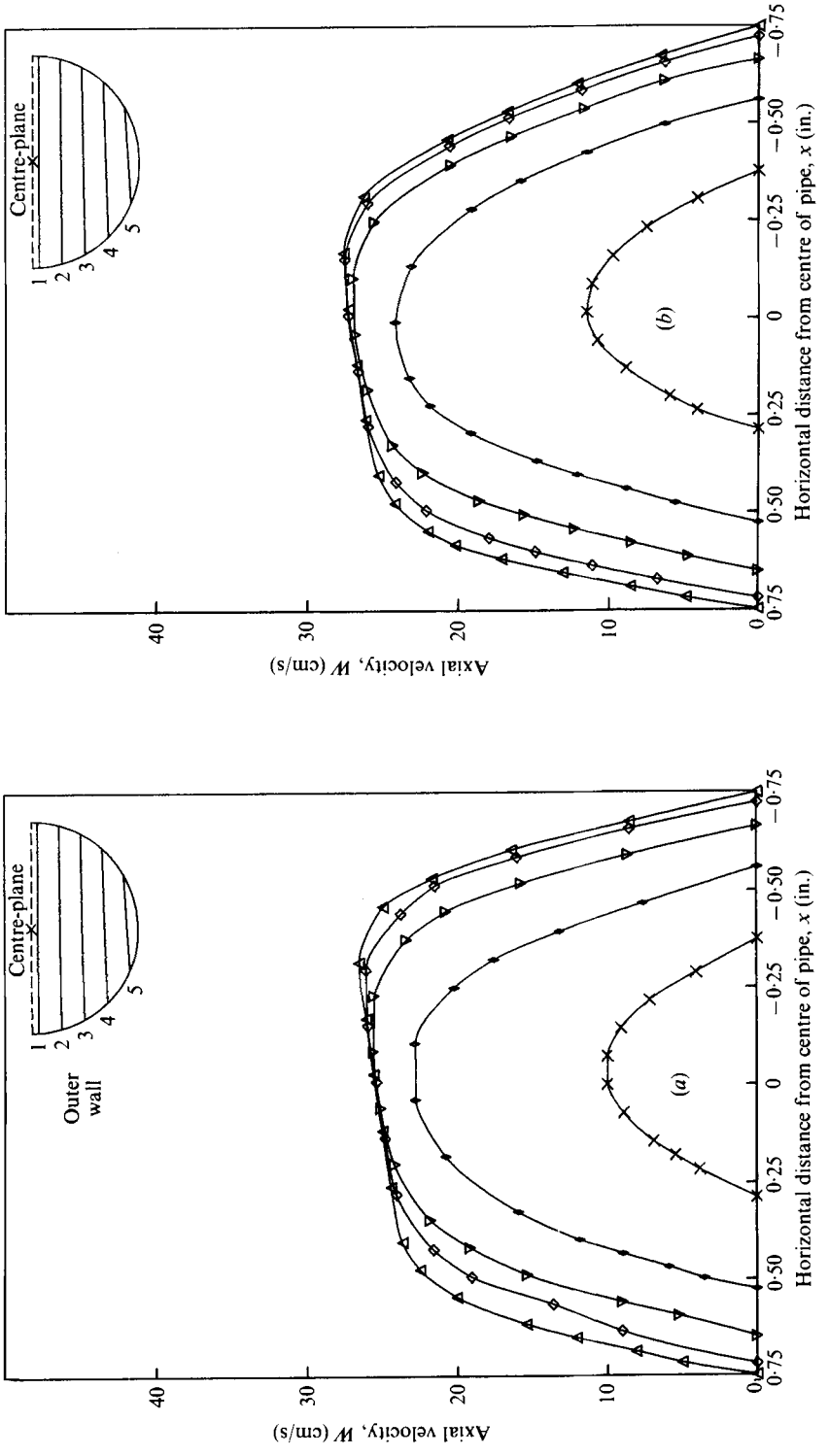

FIGURES 6(*a*, *b*). For legend see p. 509.

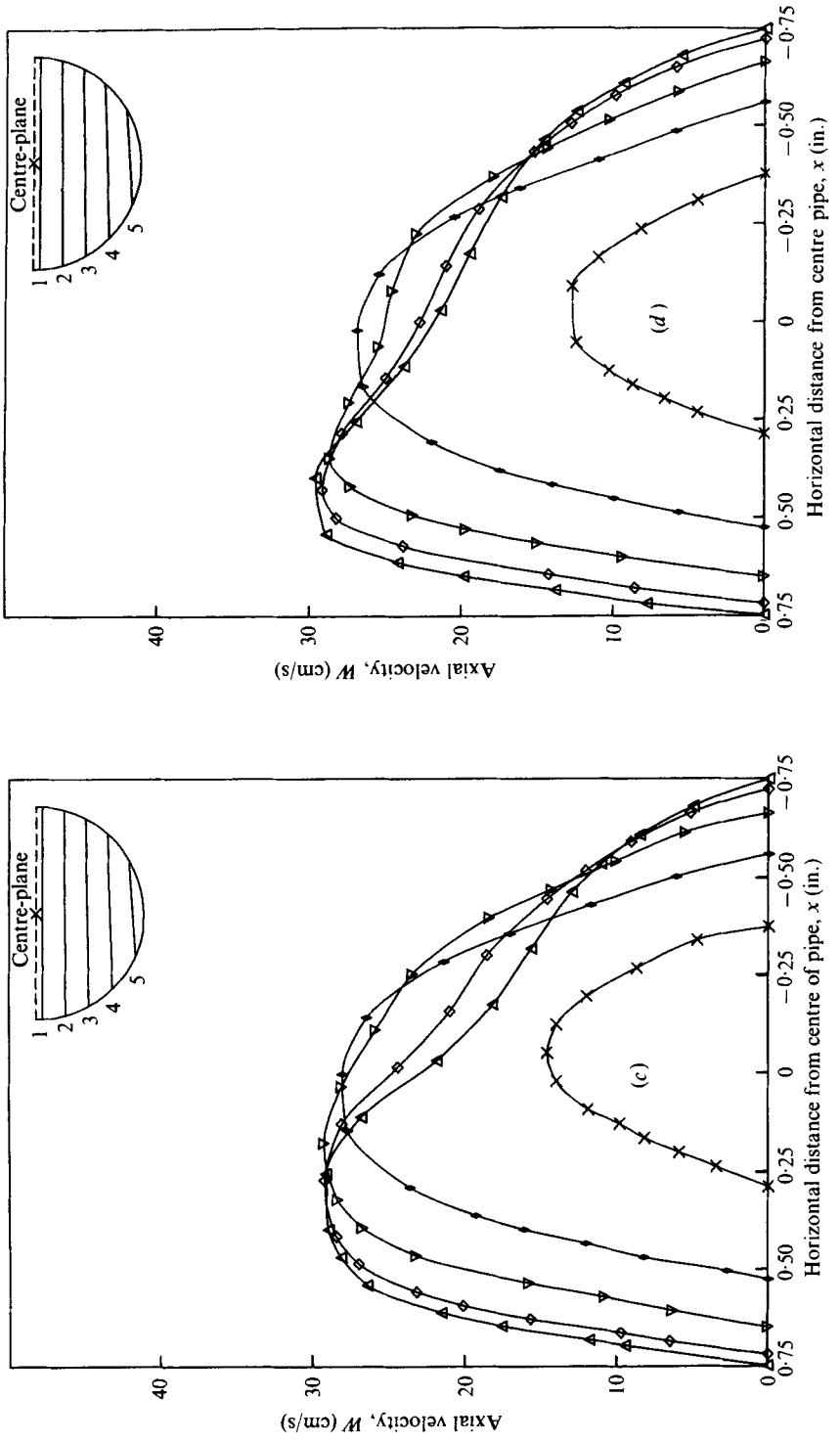

FIGURES 6(*c*, *d*). For legend see following page.

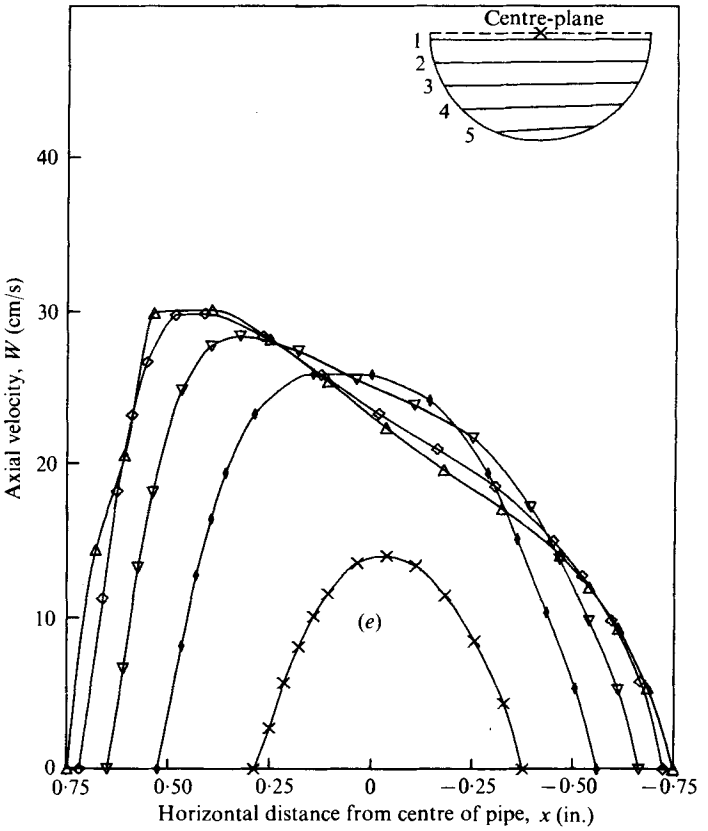

FIGURE 6. Axial velocity profiles for $\alpha = \frac{1}{7}$, $\kappa = 183$, $\overline{W} = 18{\cdot}1$ cm/s. (*a*) $l/a = 1{\cdot}84$, (*b*) $l/a = 3{\cdot}68$, (*c*) $l/a = 7{\cdot}34$, (*d*) $l/a = 13{\cdot}44$, (*e*) $l/a = 19{\cdot}54$. Profiles are shown along data lines 1–5. The initial values of y at the outer wall of the pipe for these lines, their slopes and the corresponding data symbols are: (1) Δ, $-0{\cdot}050$, $-0{\cdot}0023$; (2) $\diamond$, $-0{\cdot}200$, $-0{\cdot}0096$; (3) ∇, $0{\cdot}350$, $-0{\cdot}0183$; (4) $\blacklozenge$, $-0{\cdot}500$, $-0{\cdot}0313$; (5) $\times$, $-0{\cdot}650$, $-0{\cdot}0636$.

flow development starting from a parabolic entry profile. In addition, the same type of profiles has been observed by Pedley, Schroter & Sudlow (1971) and Brech & Bellhouse (1973) in studies of the entry region downstream of a branch in a vessel, where flows with curvature of the core-flow streamlines are similarly involved.

Flow development in the downstream region for the low-κ case is substantially the same as that for high κ, but a few qualitative differences are to be noted. Most important, the doubly peaked axial velocity profiles just discussed are not observed (see figures 6*c–e*).

Figure 7 shows a plot of the isovelocity contours constructed from the data in figure 5 (*c*) ($\kappa = 565$, $l/a = 29{\cdot}4$). One observes from these isovels that the second peaks in the axial velocity profiles are due to a ridge-like zone of high axial velocity which persists in the lower part of the inner region of the pipe, although the high axial velocity fluid in the region of the midplane has shifted towards the outer wall. At low Dean numbers, the isovels in the core region are more or less vertical and do not double back on themselves, thus the second maxima do not appear.

In figure 8 the axial velocity profile measured close to the plane of symmetry (data line 1) for the case $\alpha = \frac{1}{7}$, $l/a = 19{\cdot}54$ and $\kappa = 372$ is compared with the fully developed

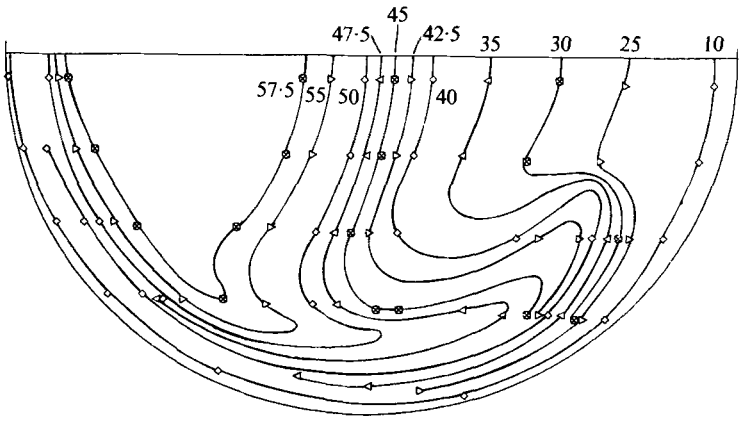

FIGURE 7. Axial isovelocity contours constructed from the data in figure 5(*c*). Numbers assigned to the isovels are the velocities in cm/s.

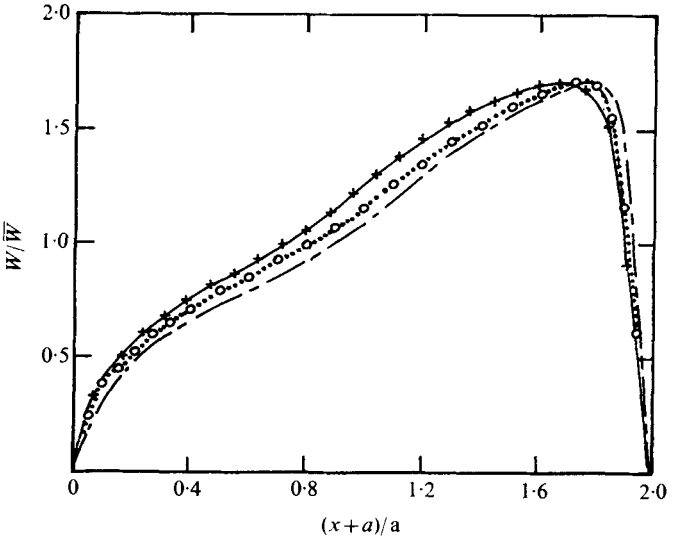

FIGURE 8. Axial midplane velocity profile comparisons. —·—, fully developed flow computed by Collins & Dennis at $\kappa = 369{\cdot}5$; o ··· o, measured by Adler at $\kappa = 372$; × — ×, present measurements at $\kappa = 372$, $l/a = 19{\cdot}54$, data line 1.

flow measurements of Adler (1934) for $\kappa = 369{\cdot}5$ and the calculated results of Collins & Dennis (1975) for $\kappa = 372$. The profiles are very similar in shape, but it is evident that the flow has not yet become fully developed in the present case. The entry length l_s for a straight pipe at a Reynolds number $\overline{W}a/\nu = 492$ (corresponding to the data of figure 8) can be calculated from the results of Fargie & Martin (1971) to be $l_s/a = 0{\cdot}196Re = 96$, which is considerably greater than the value of $l/a = 19{\cdot}54$ corresponding to the present data. According to the calculations of Yao & Berger, the entry flow length l_c for flow development in a curved pipe for the conditions of figure 8 is about 10 % greater than for a straight pipe. Evidently, the final stages of flow development occur rather slowly, since although l/a is much smaller than l_s/a or l_c/a, the developing velocity profile is not much different from the fully developed one.

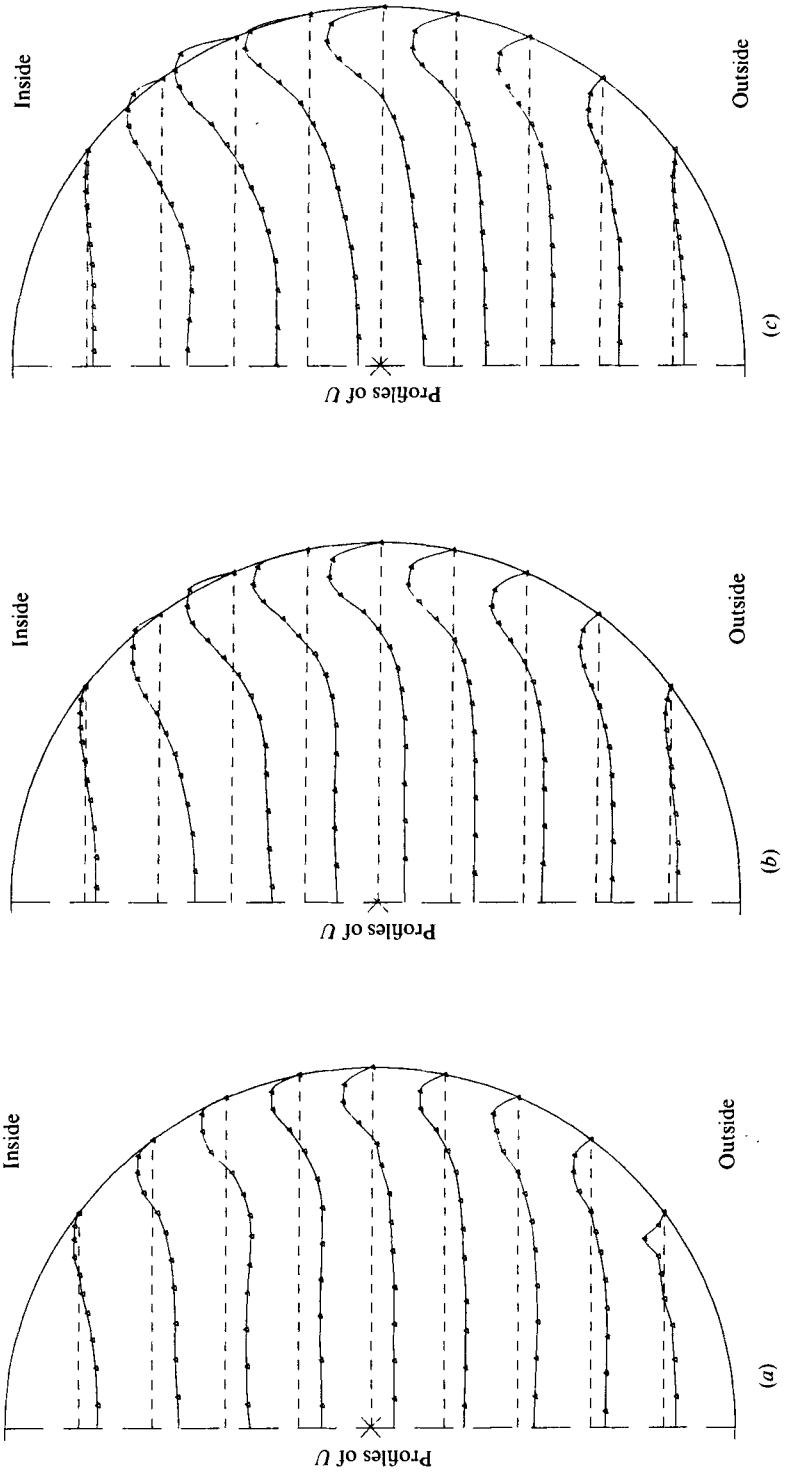

FIGURES 9(*a–c*). For legend see following page.

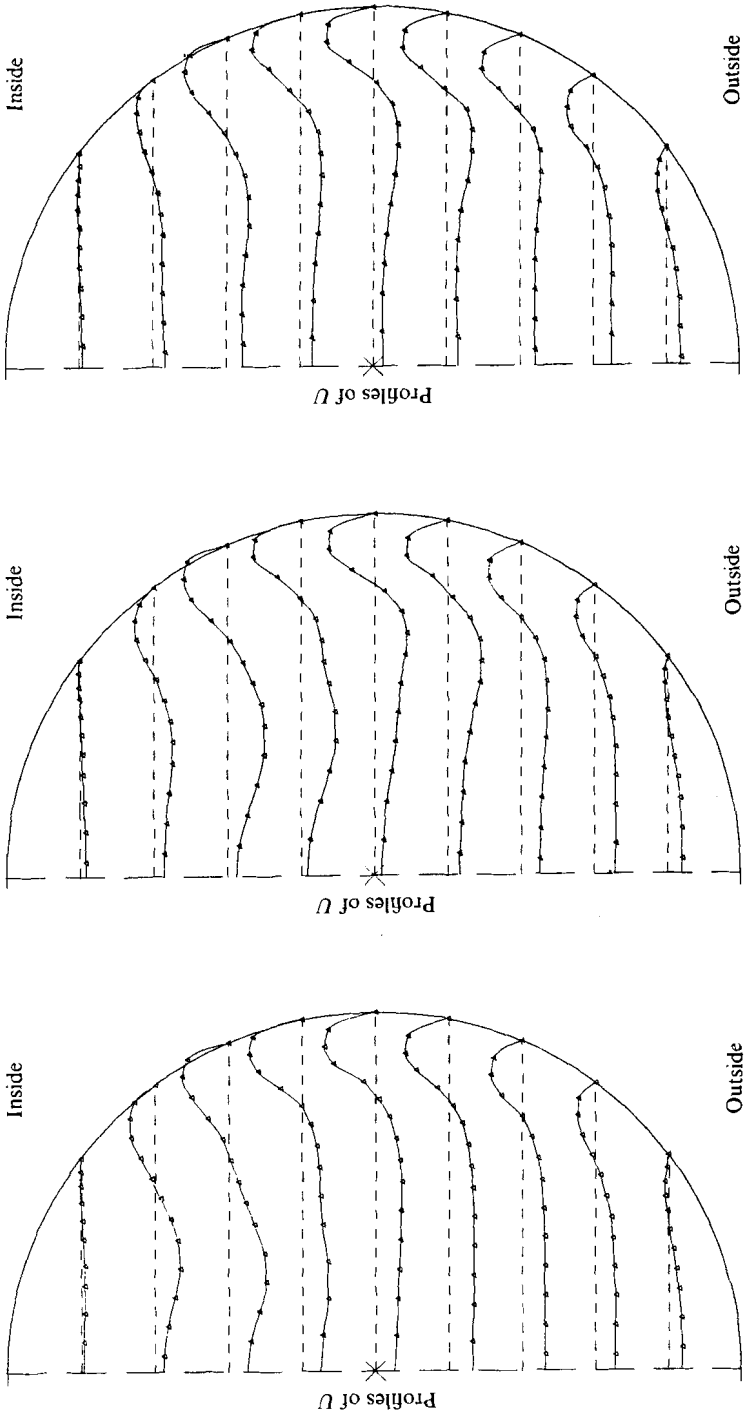

FIGURE 9. Secondary velocity profiles for $\alpha = \frac{1}{2}$, $\kappa = 138$. (*a*) $l/a = 1{\cdot}83$, (*b*) $l/a = 3{\cdot}67$, (*c*) $l/a = 6{\cdot}11$, (*d*) $l/a = 9{\cdot}16$, (*e*) $l/a = 12{\cdot}83$, (*f*) $l/a = 16{\cdot}49$. The velocities are plotted on a scale for which the distance between adjacent data lines corresponds to 5 cm/s.

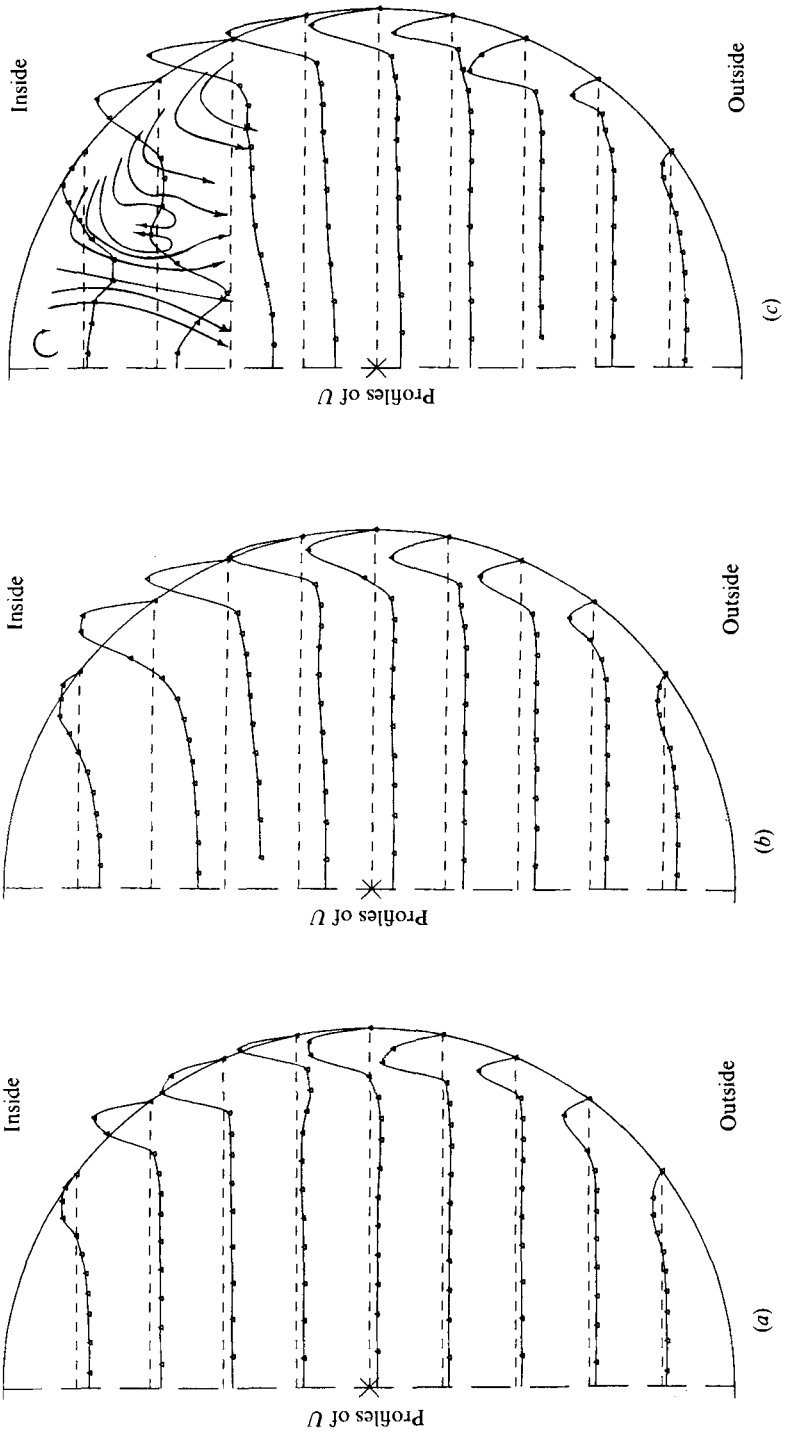

FIGURES 10(*a*–*c*). For legend see following page.

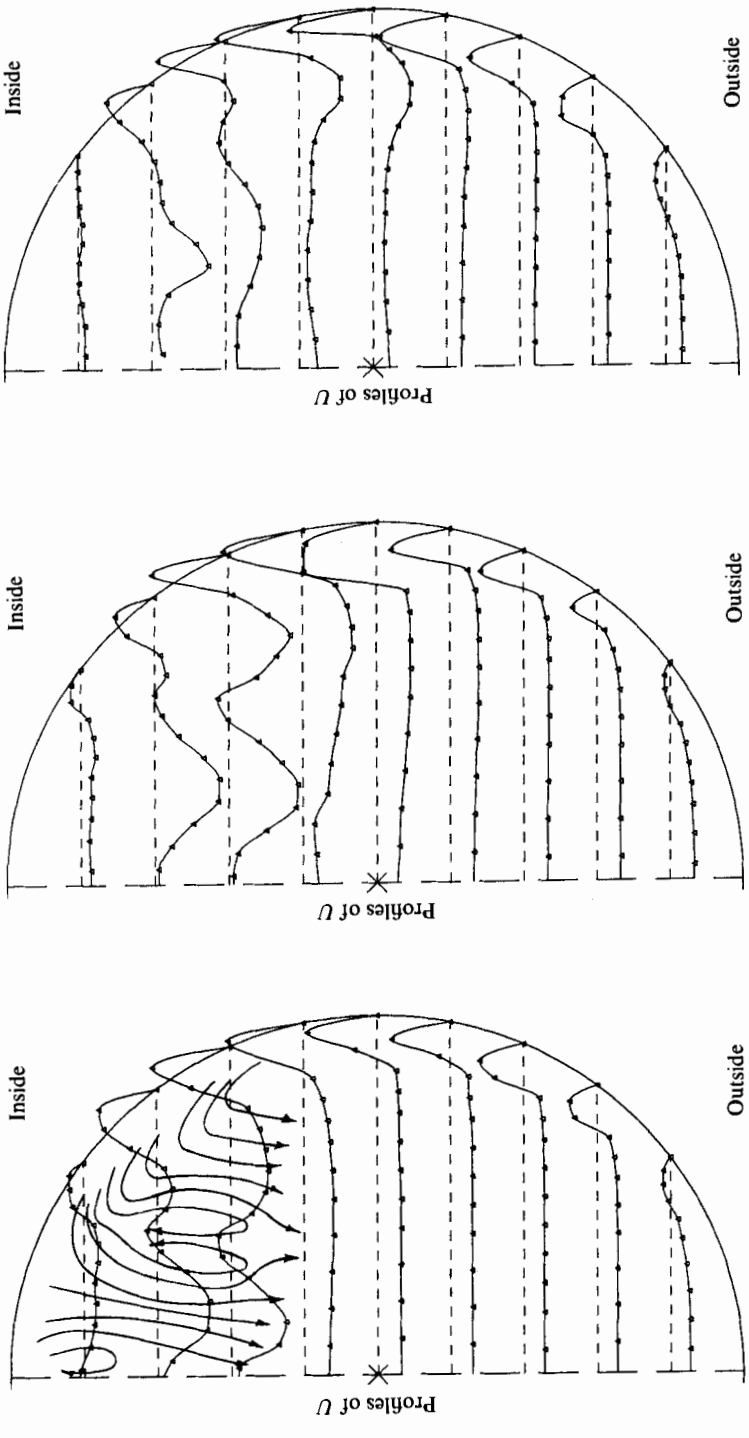

FIGURE 10. Secondary velocity profiles for $\alpha = \frac{1}{7}$, $\kappa = 678$. (*a*) $l/a = 1{\cdot}83$, (*b*) $l/a = 3{\cdot}67$, (*c*) $l/a = 6{\cdot}11$, (*d*) $l/a = 9{\cdot}16$, (*e*) $l/a = 12{\cdot}83$, (*f*) $l/a = 16{\cdot}49$. The velocities are plotted on a scale for which the distance between adjacent data lines corresponds to 10 cm/s.

We consider now the secondary velocity data, shown in figures 9 $(a)-(f)$ for $\kappa = 138$ and figures 10(a)–(f) for $\kappa = 678$, both sets of data having been obtained in the $\alpha = \frac{1}{7}$ pipe. The $\kappa = 138$ data exhibit about what one would anticipate. At the first measurement station, $l/a = 1{\cdot}83$ (figure 9a), the potential vortex has already been established, and the flow is now outward within the core and inward within the circumferential wall boundary layer. As the flow proceeds (figure 9b, $l/a = 3{\cdot}67$) the core velocity increases and the wall boundary layer thickens, and this trend is evident also at $l/a = 6{\cdot}11$, figure (9c). At $l/a = 9{\cdot}16$ (figure 9d) there is an indication that separation of the secondary flow boundary layer† may have occurred (on the innermost data line), and there is an enhancement of the outward secondary flow velocity in a region between the midplane and the pipe wall perhaps caused by the fluid returning from the wall boundary layer at the curve of separation. This behaviour is evident also at $l/a = 12{\cdot}83$ (figure 9e) and at $l/a = 16{\cdot}49$ (figure 9f). One notes that the magnitude of the outward secondary motion, as, for example, in the vicinity of the midplane, is a decreasing function of l/a in the far downstream region. This is what one expects in the flow development process. In the early stages of flow development, there must be a net outward mass flux associated with the movement of the axial velocity maximum towards the outer wall. As the flow approaches the fully developed limit, this net mass flux diminishes until finally it vanishes when the secondary flow streamlines become closed in the fully developed limit. One notes also that the maximum circumferential velocity within the wall boundary layer occurs at about $\psi = \frac{3}{2}\pi$, as anticipated on the basis of the vorticity arguments given earlier.

The secondary flow data obtained at $\kappa = 678$ (figures 10a–f) are more difficult to interpret. Although the secondary velocities at $l/a = 1{\cdot}83$ (figure 10a) and $l/a = 3{\cdot}67$ (figure 10b) exhibit the same qualitative features as are observed at the lower Dean number, namely more-or-less uniform outward motion within the core and strong inward motion within the narrow wall boundary layer, the situation changes quite dramatically further downstream. One observes additional flow reversals along the second data line (counting from the inner wall), first at $l/a = 6{\cdot}11$ in figure 10(c) and then along both the second and the third data line at $l/a = 9{\cdot}16$ in figure 10(d). The pattern persists to $l/a = 12{\cdot}83$ (figure 10e) and vestiges of it still remain at $l/a = 16{\cdot}49$ (figure 10f). It also appears from figure 10(f) that separation of the secondary flow boundary layer may have occurred at the first data line.

A possible interpretation of the flow reversals along the second and third data lines as being due to two embedded helical motions is sketched in figures 10(c) and (d). However, we have thus far been unable to devise a satisfactory explanation for their existence. Although both clockwise and counterclockwise streamwise vorticity is present in the circumferential boundary layer, as discussed in the introduction, it is not apparent how this vorticity could be the source of that contained in the embedded vortical region. Intuitively, one might expect that such motions could appear at the inner wall, as a result of separation, and indeed there is the hint of the possible exist-

† In laminar, fully developed curved-pipe flow, according to our present understanding (see Smith (1975) for a discussion of the existence of an attached flow solution for a circular cross-section) the boundary curve given by $\psi = \pi$, $r = a$ is the envelope of limiting streamlines on the inner wall. We use the term 'separation' to describe the existence of two envelopes of limiting streamlines on the inner wall symmetrically disposed about the midplane at (not necessarily constant) values of $\psi \gtrless \pi$.

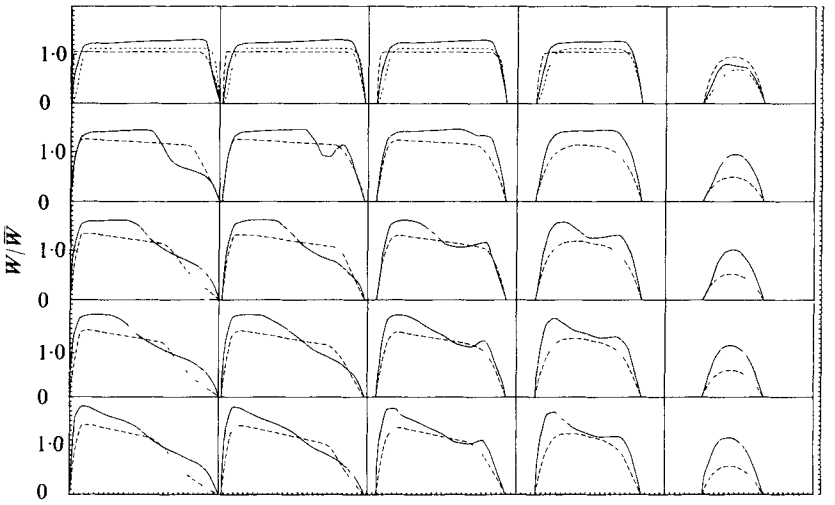

FIGURE 11. Comparisons between measured axial velocities at $\kappa = 565$, $\alpha = \frac{1}{20}$ and theoretical predictions of Singh (- - - -) and Yao & Berger (— — —). Left edge of each profile corresponds to outer wall of pipe. Profiles in a horizontal row are along data lines 1–5, from left to right, at a given l/a. The values of l/a from top to bottom are 2·4, 12·2, 29·4, 37·6 and 57·6.

ence of vortex motion, albeit very weak, in the region of the first data line in figure 10 (*d*). The embedded vortex region does coincide more or less with the ridge of high axial velocity (figure 7), and the recirculation within this region may thus be the cause of the persistence of the high axial velocity there. Evidently, if our conception of the fully developed flow is correct, both the embedded vortex region and the separated flow region must eventually be engulfed by the 'Dean-type' secondary motion. It is of interest to note that Scarton, Shaw & Tsapoges (1977) report the observation, by means of a dye flow-visualization technique, of two counter-rotating 'trapped inner wall vortices'. From the description given, it would appear that these trapped vortices are the result of flow separation.

Another interesting feature of the secondary flow field seen in figures 10 (*c*)–(*e*) is the relatively narrow region of strong outward flow above the hypothesized embedded vortex region. Conceivably this region is analogous to the 'central viscous layer' postulated by Adler and Yao & Berger, although they placed its location at the mid-plane of the pipe. A similar region, though much less pronounced, was noted for the $\kappa = 183$ data.

Comparison with theory

Axial velocity profiles were constructed from the theoretical solutions of Singh and Yao & Berger, along the data lines of our measurements, and are shown in figure 11. Since the region of validity of Singh's solution extends only a streamwise distance $O(a)$ from the entry, we have compared his results only at the first axial measurement station. The results of Yao & Berger are compared at all stations.

Evidently, Singh's solution does not predict the initial formation of the vortex-type inviscid core. This stems from the expansion procedure employed by him, where the effect of curvature appears only through a term of order $\alpha/Re^{\frac{1}{2}}$, implying uniform flow as the inviscid solution. Further, since he did not compute flow acceleration in the

core to account for boundary-layer displacement, the normalized mass flux from his profile appears to be less than unity.

It was not possible from our experiments to determine the location of the 'cross-over' point, which is the axial distance from the entrance at which the wall shear at the outer wall becomes equal to that at the inner wall, and was found by Singh to be at $z = 1{\cdot}9a$ and by Smith to be $1{\cdot}51a$, in both cases independent of Re. The velocity gradients at the inner and outer walls on data line 1 at the first measurement station for both pipes would seem to indicate that the 'cross-over' has occurred upstream of these measurement stations, in order-of-magnitude agreement with the predictions, though of course determination of wall shear by extrapolation of a velocity profile is not an accurate procedure.

The analysis of Yao & Berger predicts a slower rate of flow development than is observed, with respect to the displacement of the velocity profile maximum towards the outer wall. The flow model used by Yao & Berger involved the assumptions of linear variation with x of the axial velocity in the core and secondary flow streamlines parallel to the plane of symmetry (following the analysis of Barua (1963) for the fully developed case), and the boundary layer was calculated by a momentum-integral method. These assumptions obviously preclude the possibility of obtaining from the analysis detailed information on the velocity profiles either in the core or in the boundary layer. However, the analysis does predict separation of the secondary flow in the inner wall region as is suggested by the experiments. The integrated normalized mass flux obtained from the Yao–Berger analysis is less than unity, probably because in their mass conservation condition they use an average value for the circumferentially varying thickness of the boundary layer. Some of these shortcomings in the Yao–Berger analysis undoubtedly could be rectified so as to give improved agreement with experiment.

4. Concluding remarks

The measurement of curved-pipe entry flow reported here exhibit two features of particular interest. The first is the transition immediately downstream of the entry of the inviscid axial velocity profile from a uniform velocity distribution to a vortex-type distribution. Although a simple explanation based on inviscid flow behaviour can be given for this transition, its existence seems to have been overlooked in the analytical investigations which have been made of the entry flow problem. The second feature of interest is the observation, for the highest Dean numbers investigated, of the development in the downstream region of pronounced axial velocity maxima near the inner wall. These maxima move away from the plane of symmetry and decrease in strength as the flow proceeds downstream. They appear to be linked to the presence of an embedded vortex pair. Separation of the circumferential boundary layer on the inner wall is also indicated.

The theoretical analyses which are at present available for curved-pipe entry flow do not predict adequately the flow development process, but it is hoped that the experimental results reported here will be helpful in suggesting directions in which these analyses can be improved.

This work was supported by the National Science Foundation under grant no. ENG-73-03970. The authors are indebted to Professor S. A. Berger for many helpful discussions.

REFERENCES

ADLER, M. 1934 *Z. angew. Math. Mech.* **14**, 257.

AGRAWAL, Y. C. 1975 Laser velocimeter study of entrance flows in curved pipes. *Univ. Calif. Coll. Engng Berkeley, Rep.* FM-75-1.

AUSTIN, L. 1971 The development of viscous flow within helical coils. Ph.D. thesis, University of Utah.

BARUA, S. N. 1963 *Quart. J. Mech. Appl. Math.* **16**, 61.

BRECH, R. & BELLHOUSE, B. J. 1973 *Cardiovasc. Res.* **7**, 593.

CARO, C. J. 1973 In *Atherogenesis: Initiating Factors, Ciba Symp. (New Ser.)*, **12**, 127. Elsevier: Excerpta Medica.

COLLINS, W. M. & DENNIS, S. C. R. 1975 *Quart. J. Mech. Appl. Math.* **28**, 133.

DEAN, W. R. 1928 *Phil. Mag.* **5**, 673.

DURST, F., MELLING, A. & WHITELAW, J. H. 1972 *J. Fluid Mech.* **56**, 143.

FARGIE, D. & MARTIN, B. W. 1971 *Proc. Roy. Soc.* A **321**, 461.

FRY, D. L. 1973 In *Atherogenesis: Initiating Factors. Ciba Symp. (New Ser.)*, **12**, 93. Elsevier: Excerpta Medica.

LIGHTHILL, M. J. 1963 In *Laminar Boundary Layers* (ed. L. Rosenhead), p. 84. Oxford University Press.

PEDLEY, T. J., SCHROTER, R. C. & SUDLOW, M. F. 1971 *J. Fluid Mech.* **46**, 365.

SCARTON, H. A., SHAW, P. M. & TSAPOGAS, M. J. 1977 Relationship of the spatial evolution of secondary flow in curved tubes to the aortic arch. In *Mechanics in Engineering*, pp. 111–131. University of Waterloo Press.

SINGH, M. P. 1974 *J. Fluid Mech.* **65**, 517.

SMITH, F. T. 1975 *J. Fluid Mech.* **71**, 15.

SMITH, F. T. 1976 *Proc. Roy. Soc.* A **351**, 71–87.

STEVENSON, W. H. 1970 *Appl. Optics* **9**, 649.

VOM STEIN, H. D. & PFEIFFER, J. J. 1972 *Appl. Optics* **11**, 305.

YAO, L. S. & BERGER, S. A. 1975 *J. Fluid Mech.* **67**, 177.